Multi-Objective Optimal Design and Current Waveforms Control of Axial-Flux Brushless DC Wheel Motors for Electric Vehicles

Yee-Pien YANG[1], Member, IEEE, Yih-Ping LUH, Cheng-Huei CHEUNG, Jui-Ping WANG, Shang-Wei WU

[1]Department of Mechanical Engineering, National Taiwan University, Taipei, Taiwan, Republic of China,
email: ypyang@ccms.ntu.edu.tw.

***Abstract*—A multi-objective optimal design of a brushless dc disc-type axial-flux wheel motor and its optimal current waveforms are presented in this paper. This dedicated motor is modeled in magnetic circuits, and designed to meet the specifications of an optimization scheme, subject to constraints, such as limited space, current density, flux saturation and driving voltage. The torque-oriented optimization is then performed to obtain the optimal current waveform subject to various constraints for the independent winding structure. The best optimal waveform with maximized torque and confined ohmic loss is found to be proportional to the magnetic flux variation in the air-gap between the stator and the rotor, which is verified the same shape as the back emf.**

***Index Terms*—axial-flux wheel motor, optimal design, optimal driving waveform, electric vehicle.**

I. INTRODUCTION

A growing interest in electric vehicles (EVs) has driven researchers and engineers to develop more efficient and reliable power systems under the pressure of the protection of natural environment. Traditional power systems for EVs are composed of batteries, electric motors with drives, and transmission gears to wheels. Each subsystem converts chemical, electrical or mechanical energy into different forms, consuming energy through the dissipation components of windage and friction. It is quite essential for engineers to look for an approach to improve the overall efficiency of electric vehicles, and hence to increase their driving range. In addition to new battery technologies, new concepts for the design of motors and their optimal driving pattern have attracted substantial attention for the improvement of overall efficiency and reliability of EVs.

Optimal control waveforms have attracted considerable attention from researchers and engineers for a variety of electrical motors. Two classes of principal objectives on the optimal design of current waveforms, namely, the maximization of efficiency with ripple free [1-3], and the maximization of torque with minimum ohmic loss [4-6] are often referred. The features of the above motors are three-phase, low rated power and low rated torque, and the ripple-free torque and efficiency are their major concerns for optimization. However, the principal requirement for the dedicated wheel motor of electrical vehicles in this paper is the maximum torque with acceptable ripples, resulting from inherent cogging torque, reluctance torque and harmonics of driving currents. If the motor has been designed with small cogging and reluctance torques, only the mutual torque is to be considered in the optimization procedure for current waveforms. It is necessary that the current profile be in phase of the back electromotive force (emf) for the optimization in terms of minimized loss, maximized efficiency, and maximized torque per ampere. In addition to synchronization, the best optimal waveform for maximized torque with confined ohmic loss was found and proved proportional to the magnetic flux variation in the air-gap between the stator and the rotor [4]. Verl and Bodson [5] proposed that the maximized torque was achieved by the optimal transition among three speed ranges for PM synchronous motors in the presence of voltage and current constraints throughout the speed range. The optimal lead angles for field weakening current were also obtained. In Ohm's research [6], an algorithm was developed to find the optimal advance angle of the desired stator current command for PM synchronous motors, where the torque production was estimated by about 15% increments. However, most optimal current waveforms were based on the conventional assumption of motors that their back emf was square, trapezoidal or sinusoidal, due to the lack of design information on the shape of the magnetic filed flux distribution in the air gap between the rotor and the stator.

This paper explores the same optimization technique reported in [4], and extends the implementation to the four-, instead of, three-phase wheel motor. The switching between the parallel and series winding connection is also discussed for high and low speed driving patterns. Section 2 reviews the four-phase wheel motor structure and its multiobjective optimal shape design. Section 3 introduces its magnetic circuit model and torque equation. The optimization technique for optimal current waveforms is addressed in section 4. Section 5 presents the drive and control implementations. A summary and concluding remarks are given in section 6.

II. MOTOR STRUCTURE AND OPTIMAL DESIGN

The four-phase disc-type axial-flux wheel motor was designed by the multi-objective optimization system tool. The rotor disc of the hub-in motor has 18 magnets to form a four-phase motor. The rotor is sandwiched between two stator plates, each with 24 teeth; their winding coils are independently wired on stator poles and grouped according to the type of motors. The motor, its drive and coil structure are depicted in Fig. 1. The ND27SH NbFeB magnet is used, which has the remanence of 1.05 Tesla and coercivity of 9.5 kOe. The laminated electrical steel sheets 35RM230 (0.35mm) have a core loss of 2.2 W/kg at 1 Tesla and 100 Hz, with their saturation flux density is between 1.4 and 1.9 Tesla.

0-7803-7912-8/03/$17.00 © 2003 IEEE

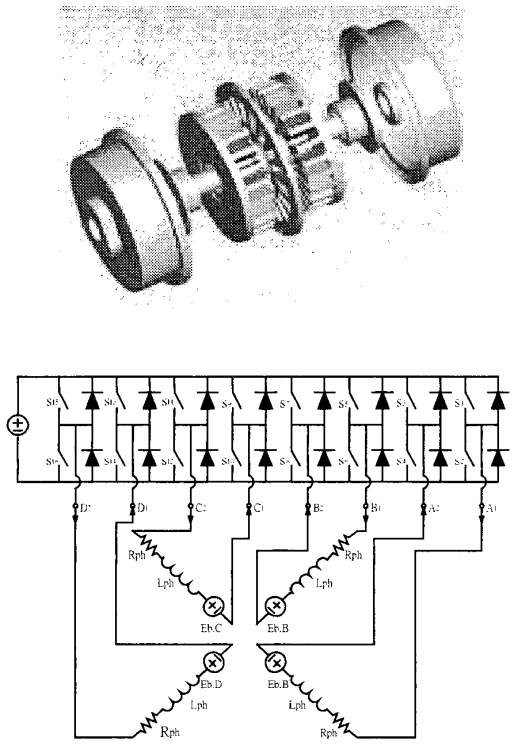

Fig. 1 The motor, drive and coil structure

The compromise programming method in the multi-functional optimization system tool (MOST) [7] is applied to search for the optimal values of the design variables that maximize the following performance indices:

Motor torque:

$$\max \quad T(s) \tag{1}$$

Torque density:

$$\max \quad T(s)/W \tag{2}$$

Motor efficiency:

$$\max \ eff = \frac{T\omega_m}{T\omega_m + P_r + P_{cl} + P_s} \bullet 100\% \tag{3}$$

in which W is the weight of the motor, P_r is the ohmic loss, P_{cl} is the core loss, and P_s is the stray loss, composed of windage, friction, noise and other less dominant loss components. The general formulations of the compromise programming method are described in Appendix A. The optimizer weighs these performance indices to reach a satifactory compromise among the design variables under the prescribed constraints:

(1) The motor dimensions must be realized.
(2) The permeance coefficient of permanent magnets $P_c > 4$.
(3) The slot current density is less than 9×10^6 (A/m^2).
(4) Conductor packing factor $k_{cp} < 0.42$.
(5) The slot opening is 1.8 times larger than the air gap length.
(6) The peak value of back emf per phase should be less than the component of the driving voltage along the back emf vector.
(7) The slot opening is 0.35 times less than the slot pitch.
(8) The flux density in electrical steel is less than its saturation value 1.8 T.
(9) The shoe fraction is confined between 0.25 and 0.5.

The optimizer MOST can deal with real, integer, and discrete design variables simultaneously. In this design, the number of stator poles, the number of winding layers and the number of turns per layer are integer design variables, while the wire diameter provided by manufactures is a discrete design variable. The optimization design of the motor was done in the following process. First, a set of initial guess of parameters was given. Second, the values of penalty functions and their corresponding gradients were calculated under the prescribed constraints. After searching along the maximum descent direct of the gradient, the next set of design parameters was determied. The convergence and constraint conditions were examined iteratively until the design was satisfactory. Its primary components and specifications are listed in Table I.

TABLE 1: SPECIFICATIONS OF THE FOUR-PHASR MOTOR

Rated speed	500 rpm	Maximum speed	1200 rpm
Rated current	15A/phase	Max. current	54A /phase
Rated torque	3 kg-m	Max. torque	6 kg-m
Rated power	1500 W	Max. power	3000 W
Outer radius	89 mm	Inner radius	56.5 mm
Air gap length	0.9 mm	No. of coils	148 / tooth
Coil diameter	0.8 mm	Motor length	95.7 mm

III. Magnetic Circuit Model and Torque Equation

Electric motors convert electrical energy to mechanical energy through a magnetic field in which the magnetic energy is stored, and the rate of change of field energy produces torque. Both the assumptions of the linearity and effective air gap of the magnetic materials are made for facilitating the modeling of the magnetic circuits. The 3D motor structure is also simplified to a 2D configuration as shown in Fig. 2, and its magnetic circuit model is illustrated in Fig. 3. In a section of 360 electrical degrees, eight teeth on each side of the stator face towards six permanent magnets embedded in the rotor. It is interesting to notice that the first four stator teeth faces the first three magnets in the order of N, S, and N, while the second four stator teeth faces instead the magnets in the direction of S, N, and S. This configuration must result in four pairs of anti-symmetric flux distributions for eight phases. Therefore, the eight-phase motor can be driven by four-phase current waveforms by a reverse winding connection for the second four stator teeth. That way this dedicated wheel motor is regarded a four-phase motor.

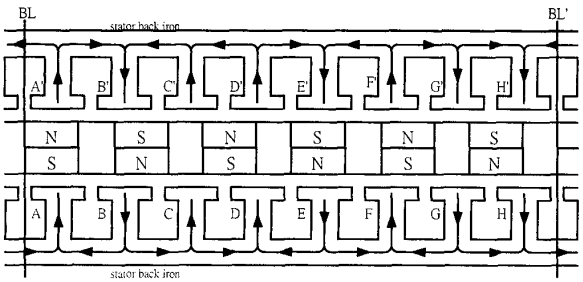

Fig. 2 2D configuration of the stator and rotor

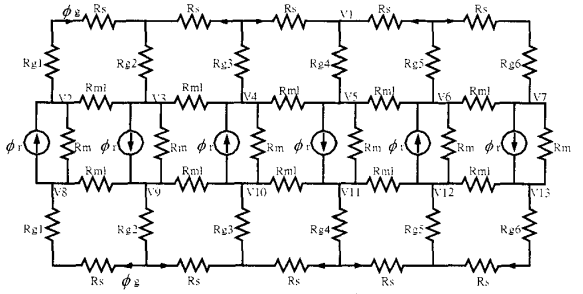
Fig. 3 Magnetic circuit model for Fig. 2

In the following magnetic circuit model, the eight-phase configuration is kept for facilitating the analysis, and the anti-symmetry of the flux distributions and the corresponding phase currents between winding phases can be present. The flux is assumed to flow straightly across the air-gaps between the stator and rotor, namely the overlapping area method, to ignore the fringing flux for simplified magnetic analysis. The relative position and magnetic flux distribution between the stator and rotor vary periodically.

The field coenergy within the air-gap is expressed in the form

$$W'(\theta)=\frac{1}{2}\sum_{i=a,b,\ldots,h}\left[(R_{g_i}+R_m)\phi_{gi}^2+L_iI_i^2+2N\phi_{gi}I_i\right] \quad (4)$$

where N is the number of turns per tooth; R_{g_i} is the air-gap reluctance corresponding to the ith coil winding; R_m is the magnet reluctance; ϕ_{g_i} is the magnet flux flowing through coil winding i; and L_i and I_i are, respectively, the phase self-inductance and the corresponding exciting current. It is apparent that R_{g_i}, ϕ_{g_i} and L_i are functions of the rotor shift, which is the relative angular position of rotor and stator; but R_m is not. The total torque consists of cogging, reluctance and alignment torques, and is obtained from the rate of change of the field coenergy in a linear operation range, as follows

$$T=\frac{\partial W'(\theta)}{\partial\theta}=\frac{1}{2}\sum_{i=a,b,c,\ldots,h}\left[-\frac{dR_{gi}}{d\theta}\phi_{gi}^2-\frac{dR_i}{d\theta}\phi_{ci}^2+2NI_i\frac{d\phi_{gi}}{d\theta}\right] \quad (5)$$

where ϕ_{Ci} is the flux produced by coil i, not by magnets, flowing through the air-gap and rotor magnets, and R_i is composed of air-gap and rotor magnet reluctances through which ϕ_{Ci} flows. The second term is the other expression of the reluctance torque due to fact of $L_iI_i^2=R_i\phi_{Ci}^2$.

In the above expression, the first term is the cogging torque produced by the rotor magnets. Since this cogging torque is inherent due to the traditional design of the motor, it is independent of the optimization of the driving currents. The second term is the reluctance torque occurring whenever the air-gap reluctance is decreasing and the inductance associated with coils is increasing. The peak ratio of the reluctance torque is less than 0.5% of the gross torque of the dedicated wheel motor, and is usually not taken into account in the optimization process. The third term, called mutual or alignment torque, happens as the mutual flux links the magnet to the coil. This is the primary torque component of brushless DC motors, and the optimal current waveform is then determined by maximizing the alignment torque

$$T_A=\frac{1}{2}\sum_{i=a,b,c,\ldots,h}NI_i\frac{d\phi_{gi}}{d\theta}. \quad (6)$$

It is important to calculate the air gap flux from six permanent magnets in an electrical period. The six magnetic sources ϕ_r yield six magnetic flux branches in the magnetic circuit model. At different position of rotor shift, the amount of magnetic flux flowing through the air gap to the facing stator teeth is assumed, for simplicity, to be proportional to the overlapping area of the magnets and the stator teeth. Therefore, the branch permeances P_{gi}, $i=1\sim6$, are defined as

$$P_{gi}=\sum_{j=a,b,\ldots,h}P_{gji}. \quad (7)$$

The node voltages V_1 through V_{13} of the magnetic circuit in Fig. 3 are then obtained by the Kirchhoff's current law and the node-voltage method, in terms of branch permeances P_{gi}, the magnet flux source ϕ_r, and the leakage permeance P_{ml}. For each rotor shift, the air gap flux of each corresponding stator teeth in an electrical period can be calculated by

$$\begin{aligned}\phi_{gi}&=(V_2-V_1)P_{gi1}+(V_3-V_1)P_{gi2}+(V_4-V_1)P_{gi3}\\&\quad+(V_5-V_1)P_{gi4}+(V_6-V_1)P_{gi5}+(V_7-V_1)P_{gi6},\\&\qquad i=a,b,\ldots,h.\end{aligned} \quad (8)$$

IV. Optimal Driving Waveform Design

The purpose of the design of the optimal current waveform is to make the most of limited battery electricity to get the maximum torque output as well as efficiency. According to the discussion in the last section, the optimal current waveform is determined by maximizing the alignment torque of the DC brushless wheel motor as expressed in (6) in the sense of average:

The average torque is maximized under a constraint on the average ohm loss. Hence, the performance index is expressed as

$$T_{A,avg}=\frac{1}{2\pi}\int_0^{2\pi}T_A(\theta)d\theta \quad (9)$$

subject to the constraint

$$\int_0^{2\pi}I_i^2d\theta\le\int_0^{2\pi}6^2d\theta,\ i=a,b,c,\ldots,h. \quad (10)$$

Both theoretical and numerical analyses are made for the

optimal current waveform with the following assumptions. First, the motor is operated under the rated speed so that the back-emf induced in each phase of the motor must not exceed the driving voltage. Second, the limitation of current and power loss of the conductor is released, which was prescribed by the maximum allowable current density of the conductor due to its cross section.

In this stage, the optimal current waveforms are obtained through a 2D magnetic circuit model as well as a 3D finite element model. The former is generated by the optimizer "constr" in MATLAB[1] for a single cost function, which is to maximize the average torque (9) over an electric period, subject to the constraint (10). The sequential quadratic programming optimization method in MATLAB is applied to search for the optimal current pattern for each phase. The optimizer "constr" in MATLAB assembles the penalty and constraint fuctions with Lagrange multipliers, and searches the stationary point of the Lagrangian function by Newton's method, Thus it is referred to as the *Lagrange-Newton* method. This method requires initial estimates for Lagrange multipliers and design variables I_a, I_b through I_h. Fig. 4 illustrates the resulting first four optimal current waveforms; the second four current waveforms are out of phase of the first four.

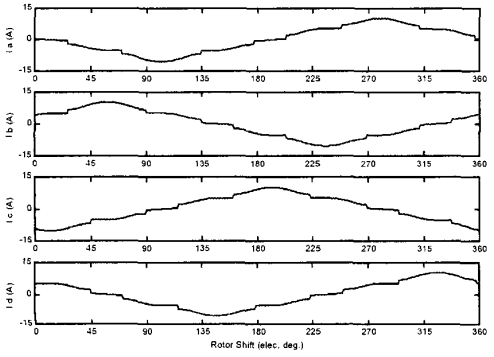

Fig. 4 Optimal current waveform from 2D magnetic circuit model.

It is well known that the torque constant of a dc motor is defined as the ratio of the produced torque and the corresponding phase current, and is the same as the electric constant as the proportional coefficient of the back emf and the motor's rotational velocity. The back emf waveform can thus be obtained by calculating the torque constant of the motor via the finite element tool ANSOFT[2] with a 3D motor model. It is interesting to find that there is no much difference between the optimal current waveform from the 2D magnetic circuit model and that in the back emf pattern from the 3D finite element model, as plotted in Fig. 5. However, the motor performance may be quite different. Through finite element analyses, the comparison of the motor performance is made not only with the optimal current waveforms created by the 2D magnetic circuit model and the 3D finite element model, but also with the square currents that is usually applied for brushless dc motors with trapezoidal back emf. For the same root mean square value of current of 6 amperes, the torque distributions with respect to the rotor shift are illustrated in Fig. 6. The average torque produced by the 3D optimal waveform, namely the back emf from the finite element analysis, is 8.03 kg-m and the best of all. The average torque driven by the 2D optimal waveform happens to be the worst among the three. This is because the simplified magnetic model had rectangular shape of magnets rather than the real trapezoidal ones in the 3D design. Linear assumptions on the materials and motor shape cause the resulting current waveform non-optimal. Its control performance is even worse then that driven by the square current waveform. Table II presents the motor performances from the numerical analysis.

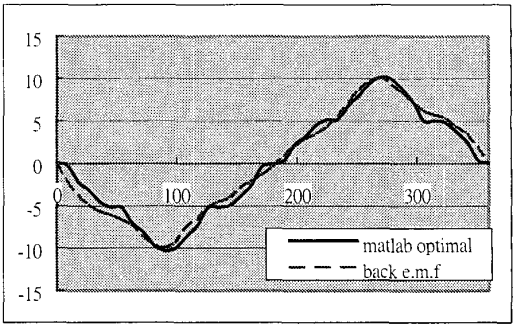

Fig. 5 Optimal waveforms by 2D (solid curve) and 3D (dashed curve) magnetic analyses

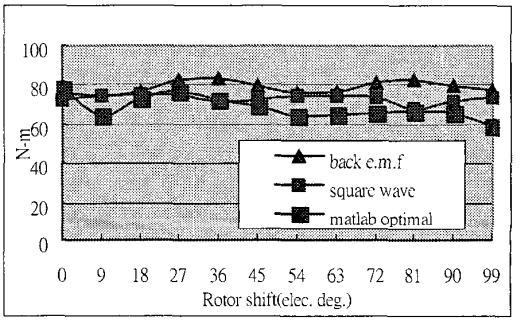

Fig. 6 Torque distributions driven by optimal currents (▲: 3D model, big ■: 2D model) and square currents (small ■)

TABLE II: Motor performance driven by various current waveforms (6 rms amp)

waveform / performance	square	2D optimal (flux variation)	3D optimal (back emf)
Average torque (kg-m)	7.45	7.06	8.03
Max. torque (kg-m)	7.67	7.98	8.48
Torque ripple (%)	3.23	13.09	5.66

V. Drive and Control Realization

Traditional PWM inverters offer the ability to change both the magnitude and frequency of the current inputs by the use of fixed DC voltage batteries on the electric vehicles. Four H-bridge inverters are used for the drive of the four-phase wheel motor, each driving an independent winding phase. The directly driven electric vehicles do not have mechanical

[1] MATLAB is a trademark of the MathWorks, Inc., Natick, Mass.
[2] ANSOFT is a trademark of Ansoft Corporation, Pittsburgh, PA

gears for the speed transition, though the electronic gear is promising alternative. The wheel motor is now installed inside the back wheel of a motorcycle, driven by four 48V batteries, each with capacity of 26 ampere-hours. The low speed or accelerating operation usually consumes larger current with lower voltage, while the high speed or cruising operation needs higher voltage but less current. Shifting the motor windings between series and parallel connections can fulfill these driving conditions. In Fig. 7, the phase current flows into the windings of the left-half stator and through the windings of the right-half stator in the series connection structure, while in the parallel connection structure the phase current flows simultaneous through both sides of the stator. The electric gear shifting circuit includes three latching relays as pictured in Fig. 8. Closing R2 with R1 and R3 open yields the series winding connection for low speed ranges; closing relays R1 and R3 with R2 open shifts to the parallel winding connection for high speed ranges. To avoid corruption of the power electronics due to short circuit by wrong switching of relays, the dead time control is implemented with an 8051 processor.

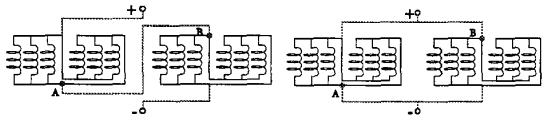

Fig. 7 Series and parallel windings

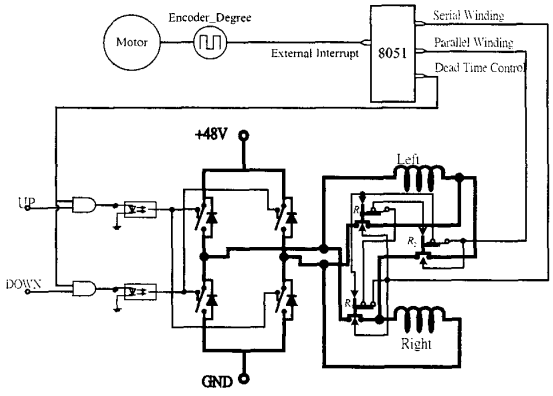

Fig. 8 Electric gear shifting circuit

The last section concludes that the optimal control waveforms in the back emf pattern by the finite element analysis provide the best motor performance in terms of produced torque. In the following performance test, three input currents are implemented. Besides the traditional square currents and the optimal current waveforms in the back emf pattern obtained by the 3D finite element model, the back emf is also extracted from experiments and implemented as the optimal shape of the driving current, as shown in Fig. 9. There seems no much difference between the currents in the back emf patterns, however the one obtained by experiment performs the best over the others as shown in Fig. 10, where the average torques are taken at various motor speeds and currents of root mean square values at 5 and 10 amperes per phase. Fig. 11 shows the efficiency curves versus motor speed where the currents in the back emf pattern from experiment again present the best performance. These curves drop down dramatically as the motor speed reaches 500 rpm, because the motor windings are connected in series and the maximum voltage is limited at 24 volts rather than 48 volts in the parallel winding connection.

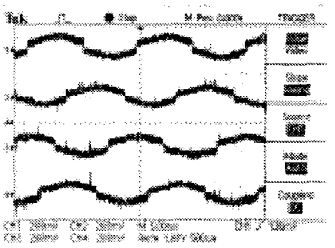

Fig. 9 Input currents of back emf pattern by experiment

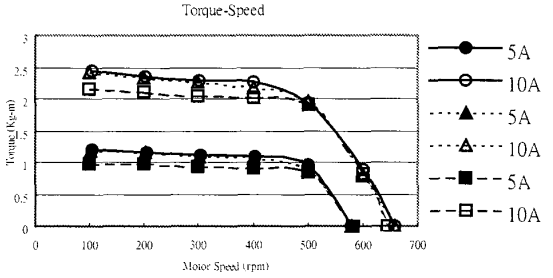

Fig. 10 Torque versus motor speed curves with current patterns of back emf wave from analysis(△▲) and experiments (○●), and square wave (■□), series winding

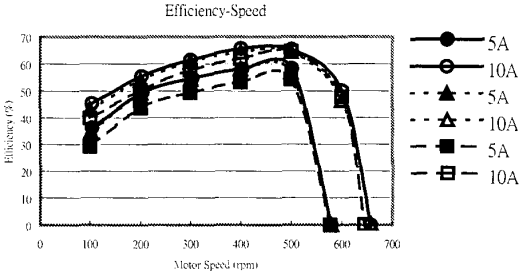

Fig. 11 Efficiency versus motor speed curves with current patterns of back emf wave from analysis(△▲) and experiments (○●), and square wave (■□), series winding

The final decision is made to implement on the electric vehicle the optimal currents in the back emf pattern obtained from experiments. Fig. 12 illustrates the torque versus speed curves for the motor wound in series, where the maximum motor speed is no more than 600 rpm, and the phase current of 30 amperes is able to generate torque about 6 kg-m over the motor speed between 200 through 400 rpm. The efficiency versus speed curves are shown in Fig. 13, where the motor operates at the maximum efficiency around 90% at the phase current of 15 amperes (rms) and the motor speed between 400 through 500 rpm. The rating of the motor thus

can be chosen at rated phase current 15 amperes, rated speed 500 rpm, rate torque 3 kg-m and rated power of 1.5 KW.

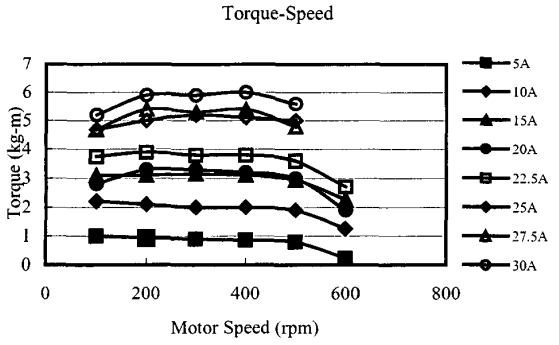

Fig. 12 Torque versus speed curves with current patterns of back emf from experiments, series winding

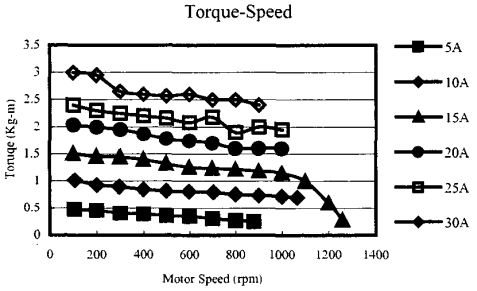

Fig. 13 Efficiency versus speed curves with current patterns of back emf from experiments, series windings.

The motor with parallel winding connections presents the other aspects on torque, efficiency and power as shown in Figs. 14 and 15. First, the motor speed reaches up to 1000 rpm due to the full 48 volts voltage across the windings. Second, the maximum torque drops to half of that gained for the motor wound in series. However, the motor cannot be driven up to 3 kg-m with the rms phase current of 30 amperes. It should be reminded that the dedicated motor is a pancake shape with a rotor sandwiched with two plates stator. Thus, one of the reasons of less torque could be the uneven current flowing to the opposite sides of the stator, whose impedances are not equal due to imperfect windings of the prototype motor. The uneven torque produced on each side of the stator drags each other, thereby deteriorating the motor performance on torque, efficiency and power.

VI. Summary and Conclusions

A dedicated optimal current waveform on the four-phase axial-flux wheel motor has been successfully designed and implemented for electric vehicles. This torque-oriented optimization with confined ohm loss leads to the optimal waveform both in-phase and proportional to the flux variation in the air-gap between the stator and the rotor. Examinations on the motor performance are made for parallel and series winding connections, respectively, for high and low speed driving patterns. The series winding connection presents better torque and efficiency than the parallel one within the motor speed of 500 rpm, while the maximum speed for the parallel winding connection reaches up to 1000 rpm. That way, the maximum driving speed of the vehicle may be reached to 70 km/hr with 70~90% efficiency for all the driving speed range. Future endeavor will be devoted to field-weakening operation, sensorless control, controller digitization, human factors, etc., to achieve better driving quality of the direct-driven electric vehicle.

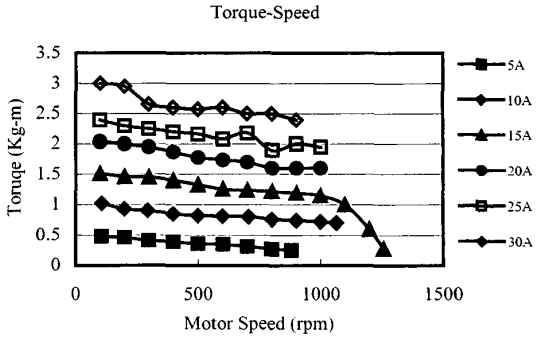

Fig. 14 Torque versus speed curves with current patterns of back emf from experiments, parallel winding

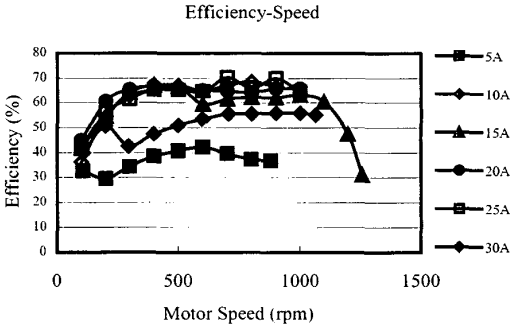

Fig. 15 Efficiency versus speed curves with current patterns of back emf from experiments, parallel winding

VII. References

[1] D. C. Hanselman, "Minimum Torque Ripple, Maximum Efficiency Excitation of Brushless Permanent Magnet Motors," *IEEE Transactions on Industrial Electronics*, Vol. 41, No. 3, June 1994, pp.292-300.

[2] S. J. Park, H. W. Park, M. H. Lee, and F. Harashima, "A New Approach for Minimum-Torque-Ripple Maximum-Efficiency Control of BLDC Motor," *IEEE Transactions on Industrial Electronics*, Vol. 7, o. 1, Feb. 2000, pp.109-114.

[3] J. Y. Hung and Z. Ding, "Minimization of Torque Ripple in Permannet Magnet Motors: A Closed Form Solution," *Proceedings of 18th IEEE Industrial Electronics Conference*, San Diego, CA, Nov. 1992, pp. 459-463.

[4] Y.-P. Yang, Y.-P. Luh, and C.-M. Lee, "A Novel Design of Optimal Current Waveform for an Electric Vehicle Wheel Motor," *Electric Power Components and Systems*, Vol. 30, No. 7, July 2002, pp.705-721.

[5] A. Verl and M. Bodson, "Torque Maximization for Permanent Magnet Synchronous Motors", *IEEE Transactions on Control System Technology*, Vol. 6, November 1998, pp.740-745.

[6] D. Y. Ohm, "Optimized Control Method Produces Maximum Torque in PM Synchronous Motors," *Powerconversion & Intelligent Motion*, Vol. 22, No. 8, 1996, pp.30-45.

[7] C.H. Tseng, W.C. Liao, and T.C. Tang, *MOST User's Manual*, Version 1.1, Technical Report No. AODL-93-01, National Chiao-Tung University, Taiwan, R.O.C., 1993.